Electron paramagnetic resonance of Gd^{3+}-doped $Dy(BrO_3)_3.9H_2$ and $Eu(BrO_3)_3.9H_2O$ single crystals: structural phase transitions and spin-Hamiltonian parameters

1992 J. Phys.: Condens. Matter 4 3659

(http://iopscience.iop.org/0953-8984/4/13/025)

J. Phys.: Condens. Matter 4 (1992) 3659–3670. Printed in the UK

Electron paramagnetic resonance of Gd^{3+}-doped $Dy(BrO_3)_3 \cdot 9H_2O$ and $Eu(BrO_3)_3 \cdot 9H_2O$ single crystals: structural phase transitions and spin-Hamiltonian parameters

Sushil K Misra and Xiaochuan Li

Physics Department, Concordia University, 1455 de Maisonneuve Boulevard West, Montreal, Quebec, H3G 1M8, Canada

Received 13 August 1991, in final form 9 December 1991

Abstract. Systematics of X-band (about 9.50 GHz) EPR measurements in the temperature range 4.2–295 K on single crystals of Gd^{3+}-doped $Dy(BrO_3)_3 \cdot 9H_2O$ and $Eu(BrO_3)_3 \cdot 9H_2O$ reveal that the $Dy(BrO_3)_3 \cdot 9H_2O$ single crystal undergoes two structural phase transitions at 67 ± 0.5 and 18 ± 0.5 K (the phase transition detected here at 18 K being the first ever reported), while the $Eu(BrO_3)_3 \cdot 9H_2O$ single crystal undergoes only one structural phase transition at 63 ± 0.5 K. The Gd^{3+} EPR spin Hamiltonian parameters at 295 and 77 K have been estimated for the two host crystals. The present Gd^{3+} EPR results on the heavier $R(BrO_3)_3 \cdot 9H_2O$ (R=Dy, Eu) crystals are found to be significantly different from those on the lighter $R(BrO_3)_3 \cdot 9H_2O$ (R=Pr, Nd, Sm) single crystals; a comparison of the features of Gd^{3+} EPR data in the lighter and heavier compounds has been provided.

1. Introduction

The paramagnetic ground state $^8S_{7/2}$ of the Gd^{3+} ion has the advantage that it readily yields well resolved EPR spectra over the entire temperature range from liquid-helium temperature (LHT) to room temperature (RT). A preliminary and inconclusive RT EPR study on Gd^{3+}-doped rare-earth bromate nonahydrate, $R(BrO_3)_3 \cdot 9H_2O$ (R≡La–Nd, Sm, Eu, Tb–Lu) (RBR) single crystals was reported by Washington (1982), which suffered from some serious shortcomings.

(i) As no angular variations in EPR line positions were recorded, it was not possible to fit the Gd^{3+} EPR line positions to a spin Hamiltonian with the correct site symmetry; a spin Hamiltonian with an axial site symmetry was assumed. (In fact, the correct spin Hamiltonian to be used is that characterized by an orthorhombic site symmetry, as discussed later.)

(ii) No detailed temperature variation study was undertaken, missing out the detection of structural phase transitions. Recently, two detailed EPR studies have been reported on Gd^{3+}-doped single crystals of RBR; specifically on $Pr(BrO_3)_3 \cdot 9H_2O$ (PrBR) by Bacquet *et al* (1990), and on $Sm(BrO_3)_3 \cdot 9H_2O$ (SmBR) and $Nd(BrO_3)_3 \cdot 9H_2O$ (NdBR) by Misra *et al* (1990). On the other hand, a preliminary EPR study on Gd^{3+}-doped $La(BrO_3)_3 \cdot 9H_2O$ (LaBR) has been published by Krygin *et al* (1988).

0953-8984/92/133659+12$04.50

The crystal structure of RBR compounds has been erroneously believed to be similar to that of the rare-earth ethylsulphate nonahydrates $R(C_2H_5SO_4)_3{\cdot}9H_2O$ (R ≡ rare earth) (RES), because the physical appearances of RBR and RES crystals are similar. The EPR of Gd^{3+}-doped RES single crystals has been extensively studied, while comparatively few studies have been published on RBR. Recent EPR observations (Bacquet *et al* 1990, Misra *et al* 1990) indicate that the Gd^{3+} EPR spectrum in a RBR host crystal is significantly different from that in a RES single crystal. In particular, when the Zeeman field B is oriented parallel to the pseudohexagonal axis, the EPR spectrum in RBR is not characterized by a mirror symmetry of the seven lines across the central line, typical of Gd^{3+} spectra in RES host crystals. (It is noted that, when B is parallel to the pseudohexagonal axis in a RBR crystal, all sections of the six hexagonal columns constituting a RBR crystal have equivalent orientations with respect to B. Thus, the EPR spectrum measured along this direction is the same as that which would be observed from a single-hexagonal column similarly oriented.) As for EPR studies of RBR single crystals doped by other rare-earth ions, EPR results on a Nd^{3+}-doped PrBR single crystal (Taylor and Sussums 1985) were not compatible with the diffraction studies (Sikka 1969, Albertsson and Elding 1977), which identified the PrBR crystal to be characterized by a hexagonal (D_{6h}^6) space group, with D_{3h} the local symmetry at the rare-earth site. However, EPR observations on Dy^{3+}- and Er^{3+}-doped $Y(BrO_3)_3{\cdot}9H_2O$ crystals at 4.2 K (Gerkin and Reppart 1987) exhibited a 60° periodicity upon rotation of B about the pseudohexagonal axis previously reported for Nd^{3+} in PrBR by Taylor and Sussum (1985). For a better understanding of the crystal structure of RBR compounds, it is helpful to know the actual symmetry at the site of the R^{3+} ion, as well as the principal values of the g-tensor of the Gd^{3+} ion used as a probe and the orientations of the principal axes of the g-tensor.

No EPR studies have so far been reported on Gd^{3+}-doped $Dy(BrO_3)_3{\cdot}9H_2O$ (DyBR) and $Eu(BrO_3)_3{\cdot}9H_2O$ (EuBR) single crystals below RT. It is the purpose of the present paper, which is a sequel to studies already reported on PrBR (Bacquet *et al* 1990), SmBR, and NdBR host crystals (Misra *et al* 1990), to report a detailed variable-temperature X-band EPR study on Gd^{3+}-doped DyBR and EuBR single crystals between LHT and RT (4.2–295 K). The values of the spin Hamiltonian parameters (SHPs) of Gd^{3+} will be determined accurately at 295 and 77 K by simultaneous fitting of all the allowed EPR line positions observed for several orientations of the external Zeeman field in the magnetic Z–Y plane, using a least-squares procedure. These values, in conjunction with the crystal-structure data, can be used for a theoretical calculation of the crystal fields experienced by the Gd^{3+} ion in the lattices of DyBR and EuBR. The systematics of the present EPR data at various temperatures will be utilized to discern the nature of the structural phase transitions undergone by DyBR and EuBR crystals. The present results on the heavier compounds DyBR and EuBR will be compared with those on the lighter compounds PrBR, NdBR and SmBR to bring out the differences between the EPR results in the heavier and lighter compounds.

2. Crystal structure, sample preparation and experimental details

A review of the crystal structure of RBR has been given by Gerkin and Reppart (1987) and has been summarized by Bacquet *et al* (1990). It is noted that RBR crystals are now generally considered to be pseudohexagonal, and not hexagonal; the latter was indicated by the neutron diffraction studies of Albertsson and Elding

(1977), and those of Sikka (1969). The pseudohexagonal structure was evidenced by optical absorption studies of Hellwege and Hellwege (1950) and those of Hellwege and Kahle (1951), and more recently by Poulet *et al* (1975). The difficulty that Albertsson and Elding (1977) encountered in detecting the twinning inherent in the pseudohexagonal structure, along with some doubt that all members of the RBR family shared this structural feature, has tended to perpetuate the idea that all RBR crystals should be quite similar to the corresponding RES crystals. This idea was later refuted by the magnetic measurements of Simizu *et al* (1984). To summarize the results of previous studies, single crystals of the isomorphic RBR compounds are biaxial and display pseudohexagonal symmetry. They contain two formula units per unit cell and are composed of six triangular sections, twinned in such a manner that the external form of the crystal is a hexagonal column, thereby giving the false impression of similarity to the RES structure. The nearest neighbours of the rare-earth (R^{3+}) ions are nine water molecules, forming a tricapped trigonal prism about the R^{3+} ion, resulting in D_{3h} symmetry at the site of the R^{3+} ion, as exhibited in figure 1. The pseudohexagonal character of RBR crystals diminishes with decreasing temperature; at about 65 K a phase transition occurs. Below 65 K, the symmetry at the site of R^{3+} ion is triclinic; there exist several physically inequivalent R^{3+} ions in the unit cell.

Single crystals of DyBR and EuBR were prepared by slow evaporation of the respective aqueous solutions, to which sufficient amounts of $Gd(BrO_3)_3 \cdot 9H_2O$ powder were added, so that one Gd^{3+} ion per 1000 Dy^{3+}, or Eu^{3+}, ions was present. DyBR and EuBR crystals were white hexagonal prisms, bounded by (100) and (101) faces.

The EPR spectra were recorded on an X-band Varian V4502 spectrometer, using a 100 kHz field modulation for RT measurements and a 200 Hz field modulation for measurements at temperatures below RT. The magnetic field was calibrated by the use of a Bruker (B-NM20) gaussmeter. For low-temperature measurements, the temperature was varied by a heater resistor inside the liquid-helium cryostat. Temperatures in the liquid-nitrogen temperature and LHT ranges were determined by measuring the resistances of platinum and germanium resistors, respectively.

3. EPR spectra

3.1. Room temperature spectra for DyBR and EuBR

The general features of the Gd^{3+} EPR spectra at RT in DyBR and EuBR are the same. The observed spectra at RT revealed the presence of two magnetically inequivalent Gd^{3+} ions for each of the DyBR and EuBR hosts. Each magnetically inequivalent Gd^{3+} ion exhibited seven allowed ($\Delta M = \pm 1$; M is the electronic magnetic quantum number) transition lines, characteristic of the electron spin $S = \frac{7}{2}$ of Gd^{3+}. When B was oriented along the crystal symmetry axis, seven lines corresponding to the transitions $M \leftrightarrow M - 1$ ($M = \frac{7}{2}, \frac{5}{2}, \frac{3}{2}, \frac{1}{2}, -\frac{1}{2}, -\frac{3}{2}, -\frac{5}{2}$) were observed. These lines were, however, not symmetrically disposed about the central $\frac{1}{2} \leftrightarrow -\frac{1}{2}$ transition for either DyBR or for EuBR. This is in accordance with the previously reported EPR studies on Gd^{3+} in PrBR (Bacquet *et al* 1990), NdBR and SmBR (Misra *et al* 1990), and LaBR (Krygin *et al* 1988) host crystals. Further, it was found, by comparison with Gd^{3+}-doped samples displaying similar angular variation of line positions, that the magnetic Z–Y plane for one of the magnetically inequivalent Gd^{3+} ions (hereafter referred to as ion I) is coincident with the most developed face, (100), of the crystal, for each of the DyBR and EuBR host crystals. At RT, the EPR spectra were recorded

for the orientations of the external magnetic (Zeeman) field B at every 2° interval in the magnetic Z–Y plane (coincident with the (100) plane of the crystal) for one of the magnetically inequivalent ions. (The magnetic X, Y, Z axes are defined to be those directions of B for which extrema in overall splitting of the lines are observed, the overall splittings being in decreasing order for $B\|Z, X, Y$, respectively (Malhotra *et al* 1976).)

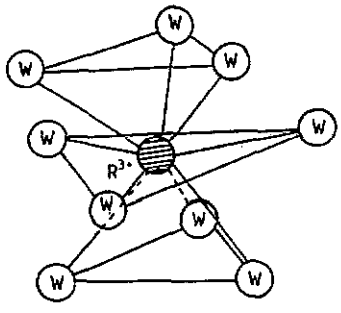

Figure 1. Coordinations of the R^{3+} (R≡ rare-earth) ion in RBR crystals at RT with the neighbouring nine water molecules (represented by W), which are its nearest neighbours.

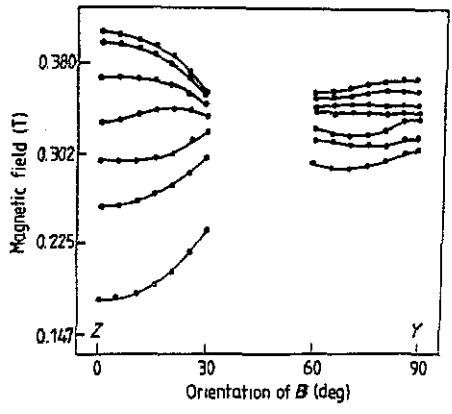

Figure 2. Angular variation in EPR line positions for Gd^{3+} in DyBR for the orientation of B in the magnetic Z–Y plane for ion I at RT: O, experimental data; —— , data points belonging to the same transition. It is difficult to discern the lines belonging to the magnetically inequivalent Gd^{3+} ion I at the orientations of B between 30° and 60° owing to overlapping by lines due to the other magnetically inequivalent ion.

The RT angular variation in the EPR line positions for Gd^{3+} in DyBR for the orientation of B in the Z–Y plane for ion I is diplayed in figure 2. The Z axes, as identified by comparison with the line positions of the EPR spectra of the respective powder samples, were found to make angles of $12° \pm 1°$ and $15° \pm 1°$ for DyBR and EuBR, respectively, with the c axis in the b–c plane; the orientations of the c axes were determined by a knowledge of the growth habits of DyBR and EuBR crystals. In the absence of an arrangement where the crystals could be rotated about two mutually perpendicular axes, it was impossible to determine the orientations of the magnetic axes corresponding to the other magnetically inequivalent Gd^{3+} ion in the unit cell. The EPR spectra at various temperatures, recorded for the orientations of B at 42° and 30° away from the principal Z magnetic axis in the magnetic Z–Y plane of Gd^{3+} ion I of DyBR and EuBR crystals, are exhibited in figure 2 and later in figure 5, respectively.

3.2. Low-temperature spectra and phase transitions

3.2.1. DyBR crystal. The temperature variation in the EPR spectrum for Gd^{3+} in a DyBR crystal, for B at 42° from the Z axis in the Z–Y plane (RT phase, for ion I), as recorded by lowering the temperature from RT (295 K) to LHT (4.2 K), is exhibited

in figure 3. It is seen from figure 3 that, upon lowering the temperature to 68 K, the general features of the EPR spectrum remained the same as those at RT. However, the overall splitting of the EPR lines increased with decreasing temperature, accompanied by broadening of the linewidths. A new spectrum, with a smaller overall splitting, appeared below $T_{c1} = 67 \pm 0.5$ K, indicating that a structural phase transition had occurred at T_{c1}. As the temperature was decreased further, the EPR lines broadened monotonically, while the intensities of the lines decreased. Below $T_{c2} = 18 \pm 0.5$ K, the line just above T_{c2} became accompanied by one more line at both lower and higher magnetic fields, implying the occurrence of another structural phase transition at T_{c2}. Below T_{c2}, the overall splitting of the line positions of the spectrum increased only slightly; also, no significant changes appeared in the spectrum down to 4.2 K. The peak-to-peak first derivative linewidths of the transition lines designated as A and B in figure 3, are plotted in figure 4 as functions of temperature in the 4.2–295 K range. These plots clearly confirm the occurrences of two structural phase transitions in DyBR at $T_{c1} = 67 \pm 0.5$ K and $T_{c2} = 18 \pm 0.5$ K.

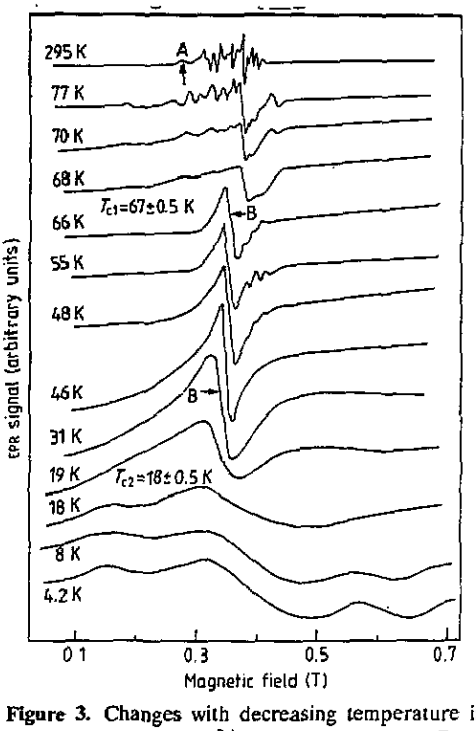

Figure 3. Changes with decreasing temperature in the first-derivative Gd^{3+} EPR spectrum in a DyBR crystal for the orientation of B at 42° from the Z axis in the Z–Y plane (RT phase, for Gd^{3+} ion I) in the temperature interval 4.2–295 K.

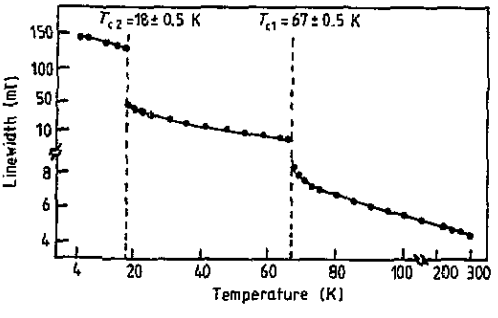

Figure 4. Temperature variations in the EPR linewidths for Gd^{3+} ion I in DyBR for the transition lines labelled as A and B in figure 3.

It is noted from figure 3 that the EPR linewidth had undergone discontinuous changes at T_{c1} and T_{c2}, implying the first-order natures of the phase transitions occurring in DyBR at these temperatures. On the other hand, the hysteresis in the values of T_{c1} and T_{c2} as found upon warming the sample is only 2 K for each phase

transition, rendering it difficult to confirm the first-order nature of these transitions as suggested by the linewidth behaviour.

3.2.2. EuBR crystal. The temperature variation in the EPR spectrum for Gd^{3+} in a EuBR crystal, for B at 30° from the magnetic Z axis in the Z–Y plane (RT phase, for ion I), as recorded by lowering the temperature from 295 to 4.2 K, is exhibited in figure 5. It was observed that, upon lowering the temperature to 64 K in steps of 5 K, the general features of the Gd^{3+} EPR spectrum in the EuBR crystal remained the same. The spectrum underwent a drastic change at $T_c = 63 \pm 0.5$ K. Below T_c, a spectrum with considerably larger overall splitting and with more lines was observed, indicating the presence of at least three magnetically inequivalent Gd^{3+} ions in the unit cell. This implied that a structural phase transition had occurred at T_c. The two phases above and below T_c coexisted over a narrow temperature range of about 2 K. Below T_c, the overall splitting of the spectrum increased monotonically with decreasing temperature; however, no significant changes appeared in the spectrum down to 4.2 K, as observed by lowering the temperature, again in steps of 5 K. Figure 6 exhibits the overall splitting of the Gd^{3+} spectrum in EuBR, for the orientation of B at 30° from the Z axis (RT phase, for ion I) in the Z–Y plane, as a function of temperature in the 4.2–295 K range, confirming the occurrence of a structural phase transition at 63 ± 0.5 K.

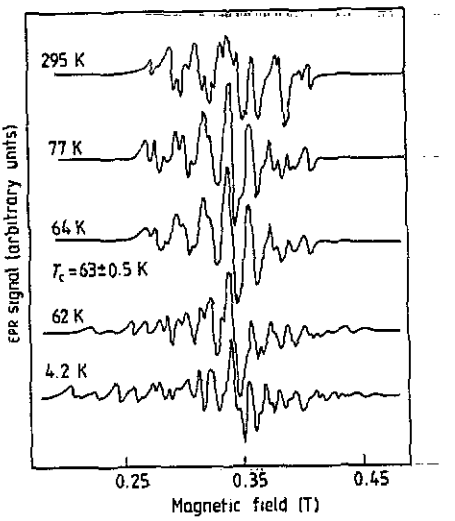

Figure 5. Changes with decreasing temperature in the first-derivative Gd^{3+} EPR spectrum in a EuBR crystal for the orientation of B at 30° from the magnetic Z axis in the Z–Y plane (RT phase, for Gd^{3+} ion I) in the temperature interval 4.2–295 K.

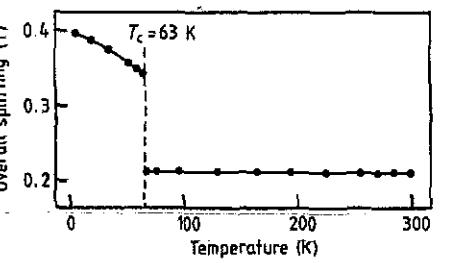

Figure 6. Temperature dependence of the overall splitting of the positions of the Gd^{3+} EPR lines in EuBR for the orientation of B at 30° from the magnetic Z axis (RT phase, for ion I).

4. Spin Hamiltonian and evaluation of parameters

A Gd^{3+} spin Hamiltonian, appropriate to an orthorhombic site symmetry, was found to fit best the Gd^{3+} allowed EPR line positions in the magnetic Z–Y plane in the

two RBR hosts investigated at present. This choice is consistent with that in other host crystals which are characterized by an orthorhombic symmetry at the Gd^{3+} site, as verified by a comparison of angular variation of line positions for rotation of B in the Z–Y plane. The spin Hamiltonian is expressed as follows:

$$\mathcal{H} = \mu_B(g_{zz}B_zS_z + g_{yy}B_yS_y) + \left(\frac{1}{3}\right)\sum_{m=0,2} b_2^{m'}O_2^m + \left(\frac{1}{60}\right)\sum_{m=0,2,4} b_4^{m'}O_4^m + \left(\frac{1}{1260}\right)\sum_{m=0,2,4,6} b_6^{m'}O_6^m. \quad (4.1)$$

In equation (4.1), μ_B is the Bohr magneton, S is the electronic spin of the Gd^{3+} ion, the O_l^m are the spin operators as defined by Abragam and Bleaney (1970), and $g_{zz}, g_{yy}, b_l^{m'}$ are the SHPs. In equation (4.1), the parameters $b_l^{m'}$ are defined in the Z–Y principal-axes system. These can be related to the parameters b_l^m, which are defined in the Z–X principal-axes system, as follows: $b_l^{m'} = b_l^m$ for all l, m except for l, 2 and l, 6 for which $b_l^{m'} = -b_l^m$. Therefore, the values of the parameters at 295 and 77 K, as listed in table 1 for Gd^{3+} ion I in DyBR and EuBR, are those of b_l^m, as deduced from $b_l^{m'}$, using these relations. (For more details on the evaluation of SHP see Misra *et al* (1990).) As for the absolute signs of the parameters, they could not be determined from the present data, since no relative-intensity data could be obtained at LHT. This is because at LHT the crystal is in a different phase (section 3.2). The sign of b_2^0 in table 1 was then assumed to be negative, in accordance with that assumed in the LaBR (Krygin *et al* 1988) and PrBR (Bacquet *et al* 1990) host crystals. The signs of the other fine-structure parameters b_l^m, relative to that of b_2^0, as yielded by the least squares fitting (LSF) procedure (Misra 1976), are, of course, correct.

It would have been interesting, in a quantitative manner, to estimate the modifications in the SHPs in passing through a phase transition. It was, however, not possible to do so with the experimental arrangement used, because it was not possible to rotate the crystal below RT around two mutually perpendicular axes to determine the orientations of the principal axes of the zero-field splitting parameter b_2^m. This information is necessary to evaluate the SHPs.

5. Gd^{3+} EPR linewidth in a DyBR crystal

The peak-to-peak first-derivative Gd^{3+} EPR linewidth, ΔB_{pp}, was found to be very temperature dependent for DyBR in the temperature range investigated, as displayed in figure 4, while ΔB_{pp} for Gd^{3+} in EuBR was comparatively much less temperature dependent. Thus, only the behaviour of the Gd^{3+} linewidth in the DyBR host crystal will be discussed at present. It was found that ΔB_{pp} depended on both the orientation and the magnitude of B. Further, ΔB_{pp} increased for any EPR line as the temperature was lowered. To give an idea of ΔB_{pp} for Gd^{3+} in DyBR in different phases, ΔB_{pp} of line A (figure 3) were measured to be 4.4 ± 0.3 mT, 7.0 ± 0.3 mT and 7.4 ± 0.4 mT at 295 K, 77 K and 70 K, respectively, and ΔB_{pp} for line B (figure 3) were measured to be 15.9 ± 0.4 mT, 28.3 ± 0.5 mT, 44.2 ± 1.0 mT, 134.5 ± 2.0 mT and 141.5 ± 2.0 mT at 46 K, 31 K, 19 K, 18 K and 4 K respectively.

The observed temperature variation in ΔB_{pp} can be related to the temperature variation in the spin–lattice relaxation time τ' of the host Dy^{3+} ions, since ΔB_{pp}

Table 1. The SHPs for Gd^{3+} ion I in DyBR and EuBR host crystals at 295 and 77 K. The g-values are dimensionless. Here SMD $(GHz^2) \equiv \sum_i(|\Delta E_i| - h\nu_i)^2$, where the summation is over the n line positions fitted simultaneously to evaluate the SHPs; ΔE_i and ν_i, respectively, are the separation of the energy levels participating in resonance for the ith line position and the corresponding klystron frequency; h is Planck's constant. The parameter errors are estimated by the use of a statistical method. The absolute sign of b_2^0 has been assumed to be negative in accordance with that in LaBR (Krygin *et al* 1988) and PrBR (Bacquet *et al* 1990) host crystals; the relative signs of all b_l^m are correct.

	DyBR		EuBR	
SHP	295 K	77 K	295 K	77 K
g_{zz}	2.0032±0.0008	2.0015±0.0009	2.0029±0.0004	1.9989±0.0003
g_{yy}	2.0033±0.0005	2.0008±0.0003	2.0029±0.0004	1.9989±0.0003
b_2^0 (GHz)	−0.4156±0.0002	−0.4454±0.0002	−0.4930±0.0002	−0.5278±0.0001
b_2^2 (GHz)	0.0228±0.0003	0.0243±0.0005	−0.0417±0.0004	0.0541±0.0003
b_4^0 (GHz)	0.0035±0.0001	−0.0031±0.0002	−0.0157±0.0003	−0.0248±0.0004
b_4^2 (GHz)	−0.1908±0.0006	−0.1766±0.0004	0.0864±0.0007	0.0769±0.0003
b_4^4 (GHz)	−0.0846±0.0006	−0.0859±0.0003	0.0194±0.0003	0.0246±0.0002
b_6^0 (GHz)	−0.0065±0.0002	0.0074±0.0004	0.0008±0.0001	−0.0101±0.0003
b_6^2 (GHz)	−0.1014±0.0003	−0.0351±0.0005	0.1072±0.0004	0.0841±0.0002
b_6^4 (GHz)	−0.0925±0.0004	−0.0659±0.0006	0.0477±0.0006	−0.0058±0.0004
b_6^6 (GHz)	0.0235±0.0002	0.0631±0.0003	−0.0442±0.0002	−0.0981±0.0002
n	98	92	98	95
SMD	0.203	0.413	0.640	0.441

is directly proportional to τ' for crystals containing two different species of paramagnetic ions, e.g. the impurity Gd^{3+} ions and the host Dy^{3+} ions in the present case. The direct proportionality between ΔB_{pp} and the spin–lattice relaxation rate τ' can be seen from the following expression derived by Misra and Orhun (1989) for the presence of two different species of paramagnetic ions, taking into account the dipolar and exchange interactions:

$$\tau' = 3g\mu_B \Delta B_{pp} f/110.45\overline{\langle\Delta\nu^2\rangle}h \tag{5.1}$$

where $f = 1.75$ for the Lorentzian lineshape and $f = 1.18$ for the Gaussian lineshape, g is the Gd^{3+} ion g-factor, μ_B is the Bohr magneton and h is Planck's constant. In (5.1), $\overline{\langle\Delta\nu^2\rangle}$ is the second moment, expressed as (Misra and Orhun 1989)

$$\overline{\langle\Delta\nu^2\rangle} = (\tfrac{1}{3})S'(S'+1)h^{-2}\left(NJ^2 + (gg')^2\mu_B^4\mu_0^2\sum_{k'}^{N}(1-3\cos^2\theta_{jk'})^2 r_{jk'}^{-6} + 2Jgg'\mu_B^2\mu_0\sum_{k'}^{N}(1-3\cos^2\theta_{jk'})r_{jk'}^{-3}\right). \tag{5.2}$$

In (5.2), J is the effective pair exchange-interaction constant between the host and impurity ions, N is the number of nearest and next-nearest neighbour ions, g', S and S' respectively, are the g-factor for the host ion, the electronic spin of the impurity ion, and the electronic spin of the host ion, $r_{jk'}$ is the vector that joins

the impurity ion to the host ion k', $\theta_{jk'}$ is the angle between $r_{jk'}$ and B, and $\mu_0 (= 1.26 \times 10^{-6} \mathrm{H\,m^{-1}})$ is the magnetic permeability constant. An examination of these expressions leads to the conclusion that the dependence of τ' on temperature T is predominantly the same as that of ΔB_{pp} on T, since $\overline{\langle \Delta \nu^2 \rangle}$, being a function of $r_{jk'}$ and J, does not depend on temperature in a drastic manner.

From the observed ΔB_{pp} versus T behaviour one can estimate the value of the power n in the power-law dependence on temperature: $\tau' \propto T^{-n}$. Accordingly, it is found that, for Dy^{3+} ions in DyBR, $n = 0.4 \pm 0.1$ for $68\,\mathrm{K} \leqslant T \leqslant 295\,\mathrm{K}$, $n = 1.2 \pm 0.1$ for $19\mathrm{K} \leqslant T \leqslant 66\,\mathrm{K}$, and $n = 0.03 \pm 0.01$ for $4\,\mathrm{K} \leqslant T \leqslant 18\,\mathrm{K}$. The well known processes, such as the Raman, the Orbach, the three-phonon, the local mode or the collision processes, for which $n \geqslant 2$ (Shrivastava 1983), do not explain the observed ΔB_{pp} versus T behaviours, since $n \leqslant 1.2$ at all temperatures in the present case. On the other hand, a satisfactory explanation of the present temperature behaviour ($n \leqslant 1.2$) may be provided by a detailed computation using the Monte Carlo technique, taking into account the dipolar interactions between the impurity ion and the host ions, in analogy to the case for Gd^{3+}-doped $Yb_xY_{1-x}Cl_3 \cdot 6H_2O$ crystals with similar T behaviours, as investigated in detail by Misra *et al* (1988).

As for the Monte Carlo computation required, the following brief set of recommended steps can be given on the spin–lattice relaxation process involving dipolar interaction between host and guest impurity ions. (For more details see the paper by Misra *et al* (1988).) A guest paramagnetic impurity ion (a Gd^{3+} ion in the present case) is assumed to be surrounded by the host paramagnetic ions (Dy^{3+} ions in the present case), with which it interacts by the dipolar interaction. The Gd^{3+} dipole moment precesses about the resultant field $B_t = B_0 + \sum_i B_i + B_{RF}$, where the dipolar fields at the Gd^{3+} site due to the Dy^{3+} neighbours are denoted by B_i, while the RF field applied at 90° to the Z axis, responsible for EPR transitions between the Zeeman levels of Gd^{3+}, rotating around the Z axis, is denoted by B_{RF}, and B_0 is the external Zeeman field directed along the Z axis. The dipole moments corresponding to the host Dy^{3+} ions are assumed to flip randomly after characteristic times, leading to a reversal in the direction of the corresponding B_i. Using $\mathrm{d}M/\mathrm{d}t = \gamma B \times M$ (where M is the magnetization), one is led to the total final magnetization

$$M'_{Tf} = M'_{Ti} - \left[\omega'_{RF} M_{z'} (\cos \phi_i - \cos \phi_f) \Big/ \left(\omega_L + \sum_j \omega_j - \omega_{RF} \right) \right] \tag{5.3}$$

where M'_T is the total magnetization, ω_L is the Larmor frequency corresponding to the precession around B_0, ω_j is the Larmor frequency corresponding to precession around B_j, ω'_{RF} is the Larmor frequency for precession around B_{RF}. The sum is over the Dy^{3+} neighbours considered and the subscripts i and f indicate the initial and final states. The full width at half-maximum (FWHM), representing the EPR linewidth, is given by the power absorbed, proportional to $M_{y'} (= M_{Tf} \sin \phi_f)$, where ϕ is the angle between M_T and the x' axis, (x', y', z') being the coordinate system rotating with the RF magnetic field responsible for resonance. In order to avoid using unknown constants the quantity $b_{y'} = M_{y'} B_{z'} / M_{z'}$, having the dimension of magnetic field, is used, where $B_{z'} = (\omega_L + \sum_i \omega_i - \omega_{RF})/\gamma$, γ $(= 2\pi g_{Gd} \mu_B / h)$ being the Gd^{3+} gyromagnetic ratio. Finally, one has $b_{y'} = \omega'_{RF} \sin(2\phi_f)/2\gamma$. A large number of $b_{y'}$ values are calculated in which the required angle ϕ_f is calculated by the Monte Carlo

technique, as follows. A uniform random-number generator is used to set initially the neighbouring Dy^{3+} dipoles up or down randomly, while a Gaussian distributed random-number generator, centred around the mean value $\mu = \tau_{Dy}$ is used to assign the characteristic times t to these dipoles with which they periodically reverse their spin directions; τ_{Dy} is the spin–lattice relaxation time of the host ions. This procedure simulates the periodic flipping of Dy^{3+} spins due to spin–lattice relaxation, especially when the computation is repeated a large number of times to generate a histogram of $b_{y'}$-values; also, it simulates the random orientations of Dy^{3+} spins. The computation of $b_{y'}$ is repeated a large number of times, e.g. 1000, for a chosen value of the ratio of relaxation times given by $R = \tau_{Gd}/\tau_{Dy}$. (R is always greater than unity since the host ions relax faster than the impurity ions.) The histogram of $b_{y'}$-values represents the EPR lineshape from which the EPR linewidth, ΔB_{pp}, can be estimated to be its FWHM. Finally, the T-dependence of the Gd^{3+} EPR linewidth is simulated by changing the value of R. A correspondence between R and T can be made so that the calculated ΔB_{pp}-values agree with the observed ΔB_{pp}-values.

6. Comparison of Gd^{3+} EPR spectra in the heavier compounds DyBR and EuBR with those in the lighter compounds PrBR, NdBR and SmBR

The general features of Gd^{3+} EPR spectra for the hosts PrBR (Bacquet *et al* 1990), NdBR and SmBR (Misra *et al* 1990), consisting of lighter rare-earth ions, are found to be significantly different from those for the hosts EuBR and DyBR, consisting of heavier rare-earth ions, as observed at present. For comparison, the RT values of the zero-field splitting parameters b_2^0 and b_2^2, the overall splittings when B is parallel to the respective magnetic Z axis for Gd^{3+} in these crystals, and the phase transition temperatures T_c, as detected from the systematics of the EPR spectra of Gd^{3+} impurity in these hosts between LHT and RT, are listed in table 2. It is seen, from table 2, that the values of the Gd^{3+} zero-field splitting parameter b_2^0 in the lighter hosts PrBR, NdBR and SmBR are roughly about four times those in the heavier hosts EuBR and DyBR, while the overall splittings of EPR lines for the Gd^{3+} ions in the lighter hosts PrBR, NdBR and SmBR are nearly three times those for the heavier hosts EuBR and DyBR. However, the magnitude of the parameter b_2^0 increased for all these hosts as the temperature was lowered. Unlike EuBR, DyBR, SmBR and NdBR crystals, which underwent phase transitions, no phase transition was detected in the PrBR crystal. More data on other lighter and heavier RBR host crystals are required, involving EPR and other techniques, in order to arrive at definitive conclusions. Further, to this end, more accurate untwinned single-crystal structural data are required, since the reported data are only on twinned crystals.

7. Concluding remarks

The main results of the present EPR study on Gd^{3+}-doped DyBR and EuBR are as follows.

(i) Two structural phase transitions have been detected to occur in DyBR at 67 and 18 K, while only one structural phase transition, at 63 K, has been observed to occur in EuBR. This may perhaps be due to the differences in the strengths of the interactions

Table 2. The RT (295 K) values of the zero-field splitting parameters b_2^0 and b_2^2, the overall splittings of Gd^{3+} EPR lines when B is parallel to the respective magnetic Z axis for Gd^{3+} in the various crystals, and the phase transition temperatures, T_c, as detected from the systematics of the EPR spectra of the Gd^{3+} impurity in the various host crystals between LHT and RT.

Host crystal	b_2^0 (GHz)	b_2^2 (GHz)	Overall splitting (T)	T_c (K)	Reference
PrBR	−1.9210	1.147	≃ 0.75	None	Bacquet *et al* (1990)
NdBR	−1.8603	1.011	≃ 0.75	29	Misra *et al* (1990)
SmBR	−1.9500	1.279	≃ 0.75	38.5	Misra *et al* (1990)
EuBR	−0.4930	0.023	≃ 0.25	63	Present work
DyBR	−0.4156	−0.042	≃ 0.25	67, 18	Present work

of the Dy^{3+} and Eu^{3+} ions with the surrounding ligands, i.e. the water molecules. The phase transitions, observed at present at 67 K for DyBR and at 63 K for EuBR, are in agreement with those detected by visible-absorption measurements on PrBR and NdBR single crystals, which exhibited a phase transition from the paraelectric to the pyroelectric phase at about 65 K (Hellwege and Hellwege 1950, Poulet *et al* 1975).

(ii) For EuBR, the angular variation in EPR line positions for B in the magnetic Z–Y plane (RT phase, for ion I) between 4.2 and 63 K indicates the occurrences of three maxima, implying, in turn, the existence of three magnetically inequivalent sites in the unit cell in the 4.2–63 K temperature range.

(iii) The SHPs for Gd^{3+} in DyBR and EuBR, for one of the two magnetically inequivalent Gd^{3+} ions in the unit cell, have been estimated at two temperatures: 295 and 77 K. The absolute value of the zero-field splitting parameter b_2^0 in each of the DyBR and EuBR host crystals, increases as the temperature is lowered. It was not possible to estimate the SHPs below the phase transition temperatures, 67 K and 63 K in DyBR and EuBR, respectively, because the crystals could not be rotated around two mutually perpendicular axes to determine the orientations of the principal axes of the zero-field splitting tensor.

(iv) The phase transition at 18 K, as detected at present in a DyBR crystal, is the first ever reported, whether by EPR or by any other technique.

(v) The EPR linewidth of Gd^{3+} in DyBR is found to be very temperature dependent. It implies that the variation in the host Dy^{3+} ions' spin–lattice relaxation time over the 4.2–295 K temperature interval may be explained by the dipole–dipole interaction.

(vi) The present Gd^{3+} EPR results for the heavier RBR compounds (R≡Dy, Eu) are found to be significantly different from those for lighter hosts PrBR, NdBR and SmBR. More EPR and structural data on RBR host crystals are required before making definitive conclusions.

It is hoped that the present EPR results will stimulate further studies on the various RBR compounds by EPR and x-ray techniques, differential scanning calorimetry, absorption measurements and other suitable techniques. These are necessary in order to understand fully the crystal fields and the nature and mechanisms of phase transitions in RBR crystals.

Acknowledgments

The authors are grateful to the Natural Sciences and Engineering Research Council of Canada for financial support (grant OGP0004485), and to the Concordia University Computer Center for providing their facilities to analyse the data.

References

Abragam A and Bleaney B 1970 *Electron Paramagnetic Resonance of Transition Ions* (Oxford: Clarendon)
Albertsson J and Elding I 1977 *Acta Crystallogr.* B **33** 1460
Bacquet G, Misra S K, Misiak L E and Fabre F 1990 *Solid State Commun.* **75** 369
Gerkin R E and Reppart W J 1987 *Acta Crystallogr.* C **43** 623
Hellwege A M and Hellwege K H 1950 *Z. Phys.* **127** 334
Hellwege K H and Kahle H G 1951 *Z. Phys.* **129** 85
Krygin I M, Prokhorov A D and Chernysh L F 1988 *Sov. Phys.–Crystallogr.* **33** 461
Malhotra V M, Bist H D and Upreti G C 1976 *J. Magn. Reson.* **21** 173
Misra S K 1976 *J. Magn. Reson.* **23** 403
Misra S K, Bacquet G and Frandon J 1990 *J. Phys.: Condens. Matter* **2** 5603
Misra S K and Orhun U 1989 *Phys. Rev.* B **39** 2856
Misra S K, Orhun U and Daniels J M 1988 *Phys. Rev.* B **38** 8683
Poulet H, Mathieu J P, Vergnat D, Hadni A and Gerbaux X 1975 *Phys. Status Solidi* a **32** 509
Shrivastava K N 1983 *Phys. Status Solidi* b **117** 437
Sikka S K 1969 *Acta Crystallogr.* A **25** 621
Simizu S, Bellesis G H and Friedberg S A 1984 *J. Appl. Phys.* **55** 2333
Taylor D R and Sussums A A F 1985 *J. Appl. Phys.* **57** 3736
Washington N M 1982 *PhD Thesis* Ohio State University